Lawrence Berkeley National Laboratory
Recent Work

Title
THE REACTION p + p ->Y + Y

Permalink
https://escholarship.org/uc/item/4c27z5h4

Authors
Button, Janice
Eberhard, Philippe
Kalbfleisch, George R.
et al.

Publication Date
1960-09-14

eScholarship.org Powered by the California Digital Library
University of California

UCRL-9347

UNIVERSITY OF CALIFORNIA

Ernest O. Lawrence

Radiation Laboratory

TWO-WEEK LOAN COPY

This is a Library Circulating Copy which may be borrowed for two weeks. For a personal retention copy, call Tech. Info. Division, Ext. 5545

BERKELEY, CALIFORNIA

DISCLAIMER

This document was prepared as an account of work sponsored by the United States Government. While this document is believed to contain correct information, neither the United States Government nor any agency thereof, nor the Regents of the University of California, nor any of their employees, makes any warranty, express or implied, or assumes any legal responsibility for the accuracy, completeness, or usefulness of any information, apparatus, product, or process disclosed, or represents that its use would not infringe privately owned rights. Reference herein to any specific commercial product, process, or service by its trade name, trademark, manufacturer, or otherwise, does not necessarily constitute or imply its endorsement, recommendation, or favoring by the United States Government or any agency thereof, or the Regents of the University of California. The views and opinions of authors expressed herein do not necessarily state or reflect those of the United States Government or any agency thereof or the Regents of the University of California.

For publication in Phys. Rev.

UCRL-9347

UNIVERSITY OF CALIFORNIA

Lawrence Radiation Laboratory
Berkeley, California

Contract No. W-7405-eng-48

THE REACTION $\bar{p} + p \rightarrow \bar{Y} + Y$

Janice Button, Philippe Eberhard, George R. Kalbfleisch, Joseph E. Lannutti
Gerald R. Lynch, Bogdan C. Maglić, M. Lynn Stevenson, and Nguyen H. Xuong

September 14, 1960

THE REACTION $\bar{p} + p \rightarrow \bar{Y} + Y$

Janice Button, Philippe Eberhard, George R. Kalbfleisch, Joseph E. Lannutti, Gerald R. Lynch, Bogdan C. Maglic, M. Lynn Stevenson, and Nguyen H. Xuong

Lawrence Radiation Laboratory

University of California

Berkeley, California

September 14, 1960

ABSTRACT

The study of the interaction $\bar{p} + p \rightarrow \bar{\Lambda} + \Lambda$, performed with the 72-inch hydrogen bubble chamber, has yielded 11 of these events in a total of 21,100 antiproton interactions at 1.61 Bev/c. The cross section for $\bar{\Lambda} + \Lambda$ production was estimated as 57 ± 18 μb. Nine of the 11 antilambdas went forward in the c.m. system. At the higher momentum of 1.99 Bev/c, one single-V and one double-V event fitting $\bar{\Lambda} + \Lambda$ production unambiguously and one single-V and one double-V event fitting $\bar{\Sigma}^0 + \Lambda$ or $\Sigma^0 + \bar{\Lambda}$ were observed in 4920 antiproton interactions. These events yield a $\bar{\Lambda}$-Λ production cross section of 55 ± 40 μb; this value is consistent with that predicted by the ratio of phase space on the basis of the 1.61 Bev/c data. No charged antisigma events were observed at the higher momentum. Three stages of particle separation utilizing velocity-selecting spectrometers were employed. At the lower momentum, background pions were one-third as numerous as antiprotons at the bubble chamber and the flux of antiprotons was about one per picture. At the higher momentum, the background pion to antiproton ratio was 1.8, and the flux of antiprotons was one every 13 pulses. Delta rays on incident interacting tracks were used to determine beam composition.

THE REACTION $\bar{p} + p \rightarrow \bar{Y} + Y^*$

Janice Button, Philippe Eberhard, George R. Kalbleisch, Joseph E. Lannutti,† Gerald R. Lynch, Bogdan C. Maglic, M. Lynn Stevenson, and Nguyen H. Xuong††

Lawrence Radiation Laboratory

University of California

Berkeley, California

September 14, 1960

I. INTRODUCTION

The study of the production and the decay of antilambdas via the reaction $\bar{p} + p \rightarrow \bar{\Lambda} + \Lambda$ was the first physics experiment performed with the 72-inch hydrogen bubble chamber. It was hoped at the outset of this experiment that the production cross section would be large enough to yield several hundred antilambda events in a reasonable length of time. The cross section has proved disappointingly small.

We have seen only 11 cases of this reaction in a total of 21,100 antiproton interactions at 1.61 Bev/c. In these events, one or both of the lambdas decayed through their charged modes. As the branching ratio of neutral to charged-plus-neutral decay is 1/3 for the lambda or antilambda, the 11 observed events should be increased by 1/8 to include the doubly neutral decay. This process is therefore 0.059% of the total antiproton interaction cross section. Using the measured total cross section of Elioff et al.,[1] we obtain $57 \pm 18\mu b$ as the cross section for this reaction.

---

* This work was done under the auspices of the U.S. Atomic Energy Commission.

† Present address: Florida State University, Tallahassee, Florida.

†† On leave from the Viet-Nam Atomic Energy Office, Viet-Nam.

Of the 11 observed events, 8 were cases in which the antilambda was produced in the forward hemisphere in the c.m. system. Figure 1 shows the first event that we obtained. Momentum and angle of production, as measured, are plotted in Fig. 2 for each of the visible lambda and antilambda decays from $\bar{p} + p \rightarrow \bar{\Lambda} + \Lambda$. Table I summarizes the results from fitting each of the 11 events by applying constraints of energy and momentum conservation. In fitting, the mass of the antilambda was assumed equal to that of the lambda; this equality is demanded by the CPT invariance of the production reaction. The events yielding charged decay of the antilambda were examined to determine the lifetime of the antilambda by a maximum-likelihood calculation. The value found was $2.8^{+1.1}_{-0.7} \times 10^{-10}$ sec. This is consistent with the prediction of equality for lambda and antilambda lifetimes, which also follows from CPT invariance of the production reaction.

The beam momentum was raised above the antisigma threshold to 2.02 Bev/c. Two events of the type $\bar{p} + p \rightarrow \bar{\Lambda} + \Lambda$, two events of the type $\bar{p} + p \rightarrow \overline{\Sigma^0} + \Lambda$ or $\Sigma^0 + \bar{\Lambda}$, and no events of the type $\bar{p} + p \rightarrow \overline{\Sigma^{\pm}} + \Sigma^{\pm}$ were observed in a total of 4920 antiproton interactions.

II. BEAM DESIGN

The lower antiproton momentum selected was 1.64 Bev/c and the higher momentum was 2.02 Bev/c. (The thresholds for production of $\bar{\Lambda}$-Λ, $\bar{\Lambda}$-Σ^0 or $\overline{\Sigma^0}$-Λ, and $\bar{\Sigma}$-Σ pairs are 1.43, 1.64, and 1.85 to 1.90 Bev/c respectively.) The "separated" beam design was patterned after the 1.17-Bev/c K^- beam of Eberhard, Good, and Ticho.[2] As the desired rejection ratio for pions relative to antiprotons was 30,000 and the distance between the Bevatron and the 72-inch chamber was about 200 ft, three separator systems were used. Each system consisted basically of two

magnetic quadrupole lenses (triplet), one parallel-plate velocity spectrometer (with crossed electric and magnetic fields), and one slit. The separation of the antiprotons from the pions was achieved by the action of these velocity-selecting spectrometers on a momentum-analyzed beam. The rejection of the vertically deflected pions was accomplished by the defining slits placed at vertical foci.

The momentum analysis was done in the horizontal median plane of the Bevatron's circulating proton beam. The negative particles were extracted from the target through a hole in the magnet yoke located 35 degrees north of the west straight section of the Bevatron (see Fig. 3). The first quadrupole (Q1) focused the target horizontally on the principal plane of the second quadrupole (Q2) (see Fig. 4). The dispersion in momentum caused by the Bevatron field was thus transformed into a spatial distribution at Q2, and the momentum bite was determined by collimation in Q2 (30 inches of uranium). The following quadrupoles (Q2 through Q6) were arranged as field lenses horizontally to give optimum transmission of the accepted momentum bite. In addition, the horizontal optics included two bending magnets (BM1 and BM2). The first was required solely to avoid a Bevatron building support column (I) in the first separator system. After the third separator system, a second bending magnet was used as a clearing field to sweep off-momentum components out of the beam in conjunction with uranium and lead collimation at the bubble chamber. The collimation was designed for a 20-degree bend.

The velocity selection was achieved in the vertical plane by deflecting the undesired pions and muons out of the horizontal plane. The parallel-plate velocity spectrometers utilize crossed electric (E) and magnetic (H) fields, with the electric field vertical and the magnetic field horizontal. With such an arrangement, particles with velocity $\beta_o = E/H$ traverse the spectrometer undeflected, whereas particles with some other velocity are deflected out of the horizontal plane by an angle

$$\Delta\theta = \frac{eV}{cp} \frac{L}{d} \Delta\left(\frac{1}{\beta}\right) \text{ radians,}$$

where p = momentum of particle in ev/c,

V = voltage applied to the spectrometer plates,

d = separation of the plates,

L = length of the plates,

and $\Delta\beta = \frac{1}{\beta_o} - \frac{1}{\beta}$, the difference in $\frac{1}{\beta}$ for the two velocities in question.

This angular separation $\Delta\theta$ was transformed into a spatial separation, S by means of the optical arrangement shown in Fig. 5.

In the vertical plane the object rays were converged to a parallel beam within the spectrometer by the first lens and then focused to an image at the slit by the second lens. (The effectiveness of each system for rejecting the undesired particles depends on the ratio of the image width W to the separation S. The width, W, is determined by target size, multiple scattering in windows, and chromatic and spherical aberrations of all electric and magnetic fields in the system.) Multiple scattering in the Bevatron exit window and the first system's entrance window, and the spherical aberrations of the first system were the most important contributions to the width W. Under typical operating conditions, the pion image had a width, W, of 0.2 in. (full width at half maximum) and had a vertical displacement, S, of 0.4 in.

The characteristics of the target, the beam, and the optical system are listed in detail for both the low-momentum and high-momentum experiments in Table II.

(Although the intensity and the transmission of the 2.00-Bev/c beam were low, significant results were obtained at this momentum. The bubble chamber exposure gave a $\Lambda\overline{\Sigma^o}$ (or $\overline{\Lambda}\Sigma^o$) event,[3] and an emulsion exposure gave a possible $\overline{\Sigma^+}$ event.[4] The 1.64-Bev/c beam resulted in the Λ-$\overline{\Lambda}$ events reported at Kiev[5] and in the more detailed report given in this paper.)

The above is a description of the beam design. The operational procedure was first to tune the system to transmit the intense pion beam as determined by measurements with a hodoscope of scintillation counters, and then to adjust the magnetic fields of the spectrometers to transmit particles with the velocity of the antiprotons.

In front of each slit was mounted a hodoscope or "sandwich" of several separate 0.20-inch-high scintillator counters. The outputs of each channel were displayed consecutively on an oscilloscope trace. When the beam was centered about the separation of a pair of adjacent counters in the sandwich, equally high traces appeared on the oscilloscope. Thus, by centering the "sandwiches" appropriately on the centerlines of the slits, the beam could be steered into each slit by adjustment of the magnetic fields in the spectrometers.

Then, upon determination of the magnetic fields required in each system for transmitting the pion beam (a) with no voltage applied to the spectrometer plates (H_o) and (b) with the desired operating voltage applied (H_π), the magnetic field H_p required to transmit the antiprotons could be calculated. This field $H_{\bar{p}}$ is given by the equation

$$(H_p - H_o) = \frac{\beta_\pi}{\beta_p} (H_\pi - H_o),$$

where β_π and β_p are the velocities of the pions and antiprotons of the beam (corresponding to the β_o defined above).

After the spectrometers were adjusted to transmit the antiprotons, the hodoscope was moved off the centerline of the slit into the rejected pion image. Complete future control over minor changes in voltages and currents was attained by adjusting them to keep the rejected image centered in the hodoscope. The intensity of the rejected image at the third slit was quite low, so that integration of the counts over several pulses was required in order to monitor the operation of the third system.

Periodically, the whole adjustment procedure was repeated in order to maintain optimum transmission over the long period of operation of this beam. (This beam setup was in use at the Bevatron for approximately five months, June through October, 1959).

III. ANALYSIS OF INTERACTIONS AND BEAM COMPOSITION

Low Momentum

The number of antiproton interactions in the chamber was determined by observing two quantities: the total number of interactions, N = 22,600, and the number of δ-rays greater than 1.0 cm in diameter (i.e., having kinetic energy greater than 3.7 Mev) on the corresponding incident tracks, N_δ = 292. (It is energetically impossible for a 1.61 -Bev/c antiproton to produce a δ-ray with energy greater than 3.7 Mev.) If we use the known cross section for production of δ-rays of >3.7 Mev by 1.5-Bev/c pions, namely 52 mb,[6] we can determine how many of the interactions were produced by pions. With correction for scanning efficiencies, this number is 3090. Since the K-meson flux is so small, we attribute the remainder of the interactions to antiprotons. We make an 8% correction to the number of antiproton interactions to take into account the fact that an antiproton scattering of less than 4.5 degrees is difficult or impossible to observe. The corrected number of antiproton interactions then becomes 21,100. If we use the total $\bar{p}$ cross section of 96 ± 3 mb[1] and take into account the 44% attenuation of the $\bar{p}$ beam in passing through the chamber, we conclude that 47,100 antiprotons were incident on the chamber. Similarly, if we use the known pion cross section[7] of 34 ± 1 mb and make an 8% correction for small-angle scatterings we find that 16,700 pions were incident on the chamber. (The effective path length was 69 in. for antiprotons and 70 in. for pions.) We determine the number of K-meson traversals by the observation of approximately 60 K^- decays in flight. Since the

probability of decay within the chamber is 15% and detection efficiency is perhaps 70%, we find that there were 600 K-meson traversals. Using the above numbers and the total numbers of incident tracks (196,000), we obtain the relative constituency given in Table II.

High Momentum

At the higher momentum, the counting of δ-rays on interacting tracks did not give a good estimate of the number of antiproton interactions, since the background pions were more numerous than the antiprotons. Also, statistics and scanning efficiency in counting δ-rays were poorer than at the low momentum. It was decided to use the number of 6-prongs to find the total number of antiproton interactions.

The fraction of antiproton interactions yielding 6-prongs was determined by separating the high-momentum film into two samples: those frames in which the antiproton time-of-flight counter coincidence registered and those frames in which it did not. (The electronic efficiency for detecting antiprotons was determined to be approximately 80%.) By assuming the various scanning efficiencies to be the same in the two samples, the ratio between the numbers of pions in the samples was obtained from the ratio of the numbers of δ-rays on interacting tracks in each. If I_B and I_A represent the total numbers of interactions in the first and second samples, respectively; if f_{Ai} and f_{Bi} represent the fraction of interactions going into channel i in each sample; and if r represents the ratio of δ-rays on interacting tracks in sample B to those in sample A; then the fraction of antiproton interactions (in either sample) going into channel i is given by

$$f_{\bar{p}i} = \frac{f_{Bi}I_B - r f_{Ai}I_A}{I_B - r I_A} .$$

The value of r was 0.42 ± 0.07. It was found that the fraction of antiprotons yielding

6-prongs was 0.061 ± 0.005. The observance of 278 6-prongs in the good film from the high-momentum run thus yielded an estimate of 4920 total antiproton interactions (with correction made for small-angle scatters). The number of background pion interactions was found to be 3570.

The antiproton total interaction cross section at 1.99 Bev/c was known to be 89 ± 4 mb[8] and the pion cross section was 31 ± 2 mb;[9] the effective path length for antiprotons and pions was 69 ± 1 in., as at the low momentum. Thus the numbers of antiprotons and pions incident on the chamber were 11,600 and 21,100, respectively. The beam constituency is given in Table II.

IV. MEASUREMENT AND FITTING OF EVENTS

Low Momentum

At the low and high momenta we measured all events that had one or two charged V decays associated with an incident track giving no charged secondaries at the point of interaction. These measurements were accomplished by use of the Franckenstein measuring projector specially designed to handle film from the 72-inch hydrogen chamber. Track coordinates measured in two of the three available stereoscopic views were read into an IBM 704 computer. A program called PANG (for momentum P and ANGle)[10] developed by Frank Solmitz, Robert Harvey, and William Humphrey performed the track reconstruction; i.e., it calculated momentum, azimuthal angle, and dip angle for each track.

Initially interactions were analyzed by plotting angles on a stereographic projection or Wulff plot and comparing values of included angle and momenta with those expected for K, Λ, or $\bar{\Lambda}$ decay and for $\bar{p} + p \rightarrow \bar{\Lambda} + \Lambda$ or $\pi^- + p \rightarrow K^o + \Lambda$, $K^o + \Sigma^o$, or $K^o + \Lambda + \pi^o$ production process. Subsequently, the IBM program known as KICK[11] (originally developed by Arthur Rosenfeld, James Snyder, and J. Peter Berge for the treatment of K-meson interactions) was utilized to fit interaction

vertices by adjusting measured quantities under constraints of energy and momentum conservation. Decay vertices were fitted, and results on the neutral tracks were passed on for fitting of the production vertex. A special type of fitting was done in the case of sigma production, for which the production and sigma-decay vertices were fitted simultaneously.

In the lower-momentum experiment, 30 double-V events and 60 single-V events were analyzed which were found to be antiproton or π-meson interactions. (Some additional ten events proved to be two-prongs, with large gaps in the incident track, or electron-positron pairs.) Events were remeasured which gave poor or ambiguous fits. The average number of measurements was two for the single V's and 2-1/2 for the double V's.

It was necessary to correct for systematic error resulting from measurement of the last bubble of the incident track as the point of interaction. Since the interaction occurred, on the average, one mean gap length beyond the last bubble, this length was added to the incident track to obtain a better estimated point of interaction; this new end point was used to correct the direction of the neutrals before the fitting of every V event.

Distribution of χ^2 for fitting of V decays and of χ^2/n for fitting production are given in Fig. 6 and 7. (In the latter expression, n is the number of degrees of freedom.) Median values of these distributions are 2 to 2.5 times as large as the expected values. The reasons for the large χ^2 values are possibly that measurement inaccuracies are underestimated, that optical distortions give errors larger than those stated by PANG (especially in dip angle), or that there may be slight magnetic field errors or turbulence effects. For each event the mean value of χ^2 from available measurements was plotted. Generally, a fit was not considered conclusive unless at least one measurement gave a χ^2 for decay of ≤ 20 and a χ^2

for production ≤ 8. In addition to the eleven cases of $\bar{p} + p \rightarrow \bar{\Lambda} + \Lambda$, 21 examples of $\pi^- + p \rightarrow K^o + \Lambda$ and 14 of $\pi^- + p \rightarrow K^o + \Sigma^o$ were found at the lower momentum. Characteristics of the $\bar{\Lambda}\Lambda$ events have been presented in Table I and in Fig. 2. The identifiable $\pi^- + p$ background events are shown on the plot of the Λ production angle versus momentum in Fig. 8. Data from both double and single vees are given.

The pi-meson momentum spectrum was found to differ greatly from the antiproton spectrum. A plot of incident momenta at the point of interaction in lambda-antilambda and six-prong events (which are produced only by antiprotons) shows a sharp momentum peak at 1610 Mev/c with a width at half-maximum of approximately ±20 Mev/c. Four-prong events and fits of $\pi^- + p$ interactions yielded an average pi meson momentum of 1470 Mev/c with considerably greater spread than that of the antiproton momentum. (See Figure 9) For many events, discrimination between antiproton or pi-meson interaction hypotheses could be made on the basis of measured beam momentum; for antiproton hypotheses, agreement within three standard deviations was demanded between the beam momentum calculated by PANG (from curvature) and the acceptable antiproton momentum of 1610 ± 32 Mev/c.

Curves drawn in Figures 2 and 8 for production angle versus momentum were calculated for an incident momentum of 1610 Mev/c for $\bar{p} + p \rightarrow \bar{\Lambda} + \Lambda$ and of 1470 Mev/c for $\pi^- + p \rightarrow K^o + \Lambda$ or $K^o + \Sigma^o$. There is considerable scattering of experimental points about the $K^o + \Lambda$ curve because of incident momentum spread.

We must estimate the probability of finding a pion reaction of the type $\pi^- + p \rightarrow K^o + \Lambda + n\pi^o$ that resembles a $\bar{p} + p \rightarrow \bar{\Lambda} + \Lambda$ reaction. It is conceivable that the K^o in the first reaction could be produced in such a direction and decay in such a manner as to look like the $\bar{\Lambda}$ in the second reaction. Pions were put through the chamber to investigate the $K^o + \Lambda + n\pi^o$ reaction; however, events from this film were few and were included with the background events plotted in Figure 8. As a result of the background study and calculations on K-meson leptonic decay,

we conclude that the probability is at most 10^{-4} that any of the 11 reactions observed could be of the type $\pi^- + p \rightarrow K^o + \Lambda + n\pi^o$.

High Momentum

The first 20% of the film taken at the higher momentum was poor because of difficulty in raising spectrometer voltages to get good separation of antiprotons from pions. The estimates of antiproton and pion interactions given above did not include this poor film. However, all double-V events and most single-V events were measured on the poor film for a study of pion background. Analysis of these high-momentum events was carried out as described above for the low-momentum events. With the exception of ten rolls (about 6000 pictures) on which single V's were not measured, all events with identifiable lambda decays from pion interactions are plotted in Figure 10. It is evident from the kinematics plot of Figs. 8 and 10 that there is much more overlap of the $\bar{p} + p \rightarrow \bar{\Lambda} + \Lambda$ with the $\pi^- + p \rightarrow K^o + \Sigma^o$ yield of lambdas at the higher momentum than at the lower momentum; thus at 1.99 Bev/c, ten single-V (lambda) K^o-Σ^o events and a few such K-Λ-$n\pi^o$ events gave spurious fits to the former reaction. One single-V antilambda from $\bar{\Lambda} + \Lambda$ production was observed. Two single-V events were found to fit lambda decay and $\Lambda + \bar{\Sigma}^o$ production; however, for these the possibility of lambda production by $\pi^- + p$ interactions could not be excluded. One single-V event was fitted as an anti-lambda from $\bar{\Lambda} + \Sigma^o$ production. One double-V event was found in which antiproton annihilation yielded antilambda plus lambda and the antilambda subsequently scattered from a target proton. (See Figure 11.) The one double-V event which fit $\overline{\Sigma^o} + \Lambda$ or $\Sigma^o + \bar{\Lambda}$ production has been reported.[3]

At the higher momentum, the cross section for $\bar{p} + p \rightarrow \bar{\Lambda} + \Lambda$ given by the above results is 55 ± 40 μb; that predicted from the 1.61 Bev/c result on the basis of phase-space increase is 100 ± 32 μb. The cross section for $\overline{\Sigma^o} + \Lambda$ and $\Sigma^o + \bar{\Lambda}$ is of comparable magnitude.

V. THEORETICAL PREDICTIONS FOR $\bar{\Lambda}\,\Lambda$ PRODUCTION

As nucleon-antinucleon interactions are not yet well understood, it is difficult to establish a good model for antihyperon-hyperon production. Comparatively little

work has been done on the latter. Cross sections as functions of antiproton energy were predicted by Domokos through comparison with antiproton scattering.[12] Frautschi has treated lambda-antilambda production by considering K-meson exchange as analogous to π-meson exchange in charge-exchange scattering.[13] In addition to this mechanism, we have considered phenomenologically nucleon core annihilation into lambda and antilambda by comparison with annihilation into two pions. Kovacs has used our experimental data to compare hyperon-pair with K-pair production on the basis of the usual statistical model.[14]

Domokos has calculated production cross sections for antihyperon-hyperon pairs obtained from antinucleon-nucleon annihilations as functions of the momentum of the incident antinucleon; he compares hyperon pair production with antinucleon-nucleon scattering to evaluate the matrix element and uses a thermodynamical method to calculate phase space. His results show little increase from 1.6 to 2.0 Bev/c; for antilambda-lambda production, fairly good agreement is obtained with the experimental value at 1.6 Bev/c.

Two possible mechanisms for antilambda-lambda production suggest themselves as consequences of conventional theories: exchange of a K-meson between nucleon and antinucleon or annihilation of antinucleon-nucleon cores.[15] The first should occur at separation distances greater than the radius of the absorbing core and can be considered analogous to antiproton-proton scattering (with diffraction scattering subtracted) or to charge-exchange scattering (see Figure 12); however, only the tail of the potential should be effective, as the K-meson Compton wavelength is very nearly the same as the estimated core radius (approximately 0.4 f). Core annihilation should occur at radii less than 0.4 f and might be compared with annihilation into two pions. For either process only very rough estimates can be made.

The cross section for K-meson exchange at 1 Bev can be calculated by comparing it with the antiproton charge-exchange cross section of 6 mb[1] and taking phase space to be proportional to the center-of-mass momentum for the two-particle final state. Thus

$$\sigma_{\bar{\Lambda}\Lambda}^{\text{exch}} \approx \sigma_{\bar{N}N} \frac{P_\Lambda}{P_N} \frac{A_\Lambda}{A_N} \cdot 1/2 \approx 6\text{mb} \cdot \frac{290}{690} \cdot \frac{A_\Lambda}{A_N} \cdot 1/2 = 1260 \frac{A_\Lambda}{A_N}\ \mu\text{b}. \quad (1)$$

The factor of 1/2 accounts for I-spin conservation; the initial antiproton-proton system is 50% in the I = 0 state and 50% in the I = 1 state, whereas the final $\bar{\Lambda}\Lambda$ system can only be in the I = 0 state. The quantity A_Λ/A_N represents the ratio of squared matrix elements for the $\bar{\Lambda}\Lambda$ -producing and $\bar{N}N$-producing exchange processes. If this quantity is ≈ 1, the estimate of $\sigma_{\Lambda\Lambda}$ is an order of magnitude larger than the experimental value; if for A_Λ/A_N a ratio of effective areas is used, with radii inversely proportional to the mass of the particle exchanged, the cross-section estimate is comparable with the observed value. If Yukawa-type wave functions are integrated over a volume outside a cylinder containing the annihilating core, the value of A_Λ/A_N is 2/3 (with the total volume integrals of K-meson and π-meson densities normalized to the same value); however, with the assumption of the K-N coupling constant to be smaller than the π-N coupling constant, this A_Λ/A_N value might be made consistent with experiment.

The cross section for producing the lambda-antilambda pair from the core depends on the total 45 mb cross section for many-pion annihilation,[16] the branching ratio into two-pion annihilation, and the relative phase-space ratio. The calculation yields

$$\sigma_{\bar{\Lambda}\Lambda}^{\text{ann}} \approx \sigma_{2n\pi}^{\text{ann}} \cdot \frac{S(2\pi)}{\sum_n S(n\pi)} \cdot \frac{P_\Lambda}{P_\pi} \cdot \frac{1}{2} \cdot 2 \cdot 3 \approx 45\text{mb} \cdot \frac{1}{600} \cdot \frac{290}{1140} \cdot 3 \approx 60\mu\text{b}. \quad (2)$$

The branching ratio for annihilation into two pions, $S(2\pi)/\sum_n S(n\pi) = 1/600$, was obtained from calculations of covariant phase space performed by B. Desai; the volume chosen was that found necessary for fitting the observed pion multiplicity in annihilations.[17, 18] The factor of 1/2 results again from I-spin conservation and the factor of 2 from pion indistinguishability; the factor of 3 is required by CP conservation. (The latter did not appear in the exchange-scattering calculation because both the processes compared led to final-state fermions; comparison of production with the production of two boson, however, demands weighting according to the number of possible transitions from the given initial states to the differing final states available.)

As the estimates given here for lambda-antilambda production are certainly not exact to better than a factor of three, it cannot be said which of the above-described mechanisms is more consistent with the experimental cross section. However, the angular distribution of antilambdas tends to favor the mechanism of K-meson exchange, as the probability is only 11% that an isotropic distribution would give forward peaking equal to or greater than that observed. It may be that the effective extent of the absorbing core which gives rise to competing annihilation processes is not well enough known to permit evaluation of the K-meson exchange.

Other calculations have been made by Dr. J. S. Kovacs. He uses the statistical model to compare antihyperon-hyperon production with annihilation processes producing a pair of K mesons. From data available on K-producing annihilation at 1.05 Bev/c[19] and preliminary estimates on K abundance in the experiment reported here, he can predict the observed antihyperon production cross section with a hyperon volume which is 0.7 times that associated with the K meson. He has also calculated the antihyperon-hyperon and K-pair abundances at higher energies.

VI. ACKNOWLEDGMENTS

We wish to thank Professor Luis W. Alvarez for his stimulation throughout this experiment and especially for his foresight and courage three years ago in initiating the construction of the 72-inch hydrogen bubble chamber.

We can hardly overemphasize the great difficulty that we faced in producing and operating this antiproton beam. We are indebted to many people who have helped solve this problem. Mr. Morris Pripstein is to be thanked for the many long hours he spent in developing and operating the beam. Dr. John Poirier, Dr. Sherwood Parker, and Mr. Keith Hinrichs and other graduate students of the Moyer group developed and operated the electronic equipment that was essential to the beam operation. The 72-inch bubble chamber crew, under the direction of Mr. J. Donald Gow and Mr. Robert Watt not only kept the bubble chamber in excellent working condition but helped with the vacuum system of the beam. Bob Watt's assistance was invaluable to the operation of the high-voltage parallel plate separators. The scanning personnel, under the direction of Dr. Hugh Bradner and Dr. Margaret Alston, has been extremely helpful in assisting with the beam development and operation as well as with the scanning. Mr. Mario Carota and Mr. George Edwards helped with the installation and engineering in the early stages of the beam development. We wish to thank the Bevatron crews for their cooperation and for their efforts in striking the internal target with the circulating beam in the very short period of time that is essential to good bubble chamber pictures. Our thanks go also to the Lofgren group who worked under adverse conditions during their experiment so that our experiment could start on schedule.

REFERENCES

1. T. Elioff et al., Phys. Rev. Letters 3, 285 (1959).
2. P. Eberhard, M. L. Good, H. K. Ticho, A Separated 1.17 Bev/c K^- Meson Beam, UCRL-8878, August, 1959.
3. J. Button et al., Phys. Rev. Letters 4, 530 (1960).
4. E. Amaldi et al., Il Nuovo cimento XVI, No. 2, 392 (1960).
5. M. L. Stevenson, 1959 International Conference on Physics of High-Energy Particles, Kiev, July 1959.
6. B. Rossi, High-Energy Particles (Prentice-Hall, Inc., New York, 1952), p. 15.
7. J. Cronin, Phys. Rev. 118, 824 (1960).
8. R. Armenteros, B. Cork, W. Wenzel, et al. (to be published).
9. D. Clark, R. Cool, and O. Piccioni, Phys. Rev. 103 1086 (1956).
10. W. Humphrey, A Description of the PANG Program, Alvarez Group Memo 111, Sept. 18, 1959, and Memo 115, Oct. 25, 1959; A. H. Rosenfeld, Digital Computer Analysis of Data from Hydrogen Bubble Chambers at Berkeley, in Proceedings of the International Conference on High-Energy Accelerators and Instrumentation, CERN 1959.
11. A. H. Rosenfeld and J. N. Snyder, Digital-Computer Analysis of Data from Bubble Chambers, IV. The Kinematic Analysis of Complete Events, UCRL-9098, Feb. 16, 1960 (to be published in Rev. Sci. Instr.); J. P. Berge, F. T. Solmitz, and H. Taft, Digital-Computer Analysis of Data from Bubble Chambers, III. The Kinematical Analysis of Interaction Vertices, UCRL-9097, March 15, 1960 (to be published in Rev. Sci. Instr.).

12. C. Domokos, Central Research Institute for Physics, Laboratory for Cosmic Rays, Budapest, Hungary (private communication).

13. S. Frautschi, University of California, Berkeley (private communication).

14. J. S. Kovacs, University of Colorado, Boulder (private communication).

15. D. B. Lichtenberg, in Midwest Conference on Theoretical Physics, Northwestern University, March, 1959.

16. On the basis of results from the experiment reported here, a breakdown of the total antiproton-proton inelastic cross section into pion production, annihilation into pions, and annihilation into K pairs plus pions will soon be published.

17. B. R. Desai, Pion Multiplicity in Nucleon-Antinucleon Annihilation, UCRL-9024, Feb. 17, 1960.

18. The experiment reported here has yielded 25 possible two-pion annihilation events, indicating an upper limit of 1 such event in 400 annihilations. Correction of systematic errors and elimination of background events should reduce this number to a value fairly consistent with the 1 in 600 quoted in the text.

19. R. Silberberg, A Further Study of Antiproton Interactions and the Annihilation Process, UCRL-9183, April 11, 1960.

FIGURE LEGENDS

Fig. 1. First example of antilambda production in the 72-inch hydrogen bubble chamber. The antilambda was produced with a momentum in the laboratory system of 750 ± 25 Mev/c; it went backwards in the center-of-mass system. The antiproton from decay of the antilambda annihilated with a target proton to produce four charged pions.

Fig. 2. Plot of production angle vs. momentum (in the laboratory system) for antilambda and lambda of the eleven events observed at 1.61 Bev/c. The scattering of some of the events results from variation in incident momentum from the front to the rear of the chamber. Values given are results from hand fits. The solid ellipses represent antilambda production; the dashed ellipses, lambda production.

Fig. 3. The beam layout. The antiprotons were produced in the target (T) by the 6.2-Bev proton beam of the Bevatron and were directed over a 200-foot path to the 72-inch liquid hydrogen bubble chamber (BC). The beam channel consisted of a "nose cone" magnetic shield (NC), six triplet 8-inch quadrupoles (Q1....Q6), two bending magnets (BM1 and BM2), three parallel-plate velocity spectrometers (SP1, SP2, SP3), and three slits (S1, S2, S3).

Fig. 4. Schematic diagram of the optics of the 1.64- and 2.02-Bev/c separated beams. The collimation in Q5 was used only in the 2.02-Bev/c beam. (The symbols shown are defined in Fig. 3; U is uranium collimation or absorber.)

Fig. 5. The optics in the vertical plane for one separator system. The angular separation ($\Delta\theta$) is transformed into the spatial separation, S. The width (W) of the image is due to the size of the object, the chromatic and spherical aberrations of the electric and magnetic fields, and the multiple Coulomb-scattering

in the windows of the vacuum systems. The ratio of W to S determines the effectiveness of the system for the rejection of the undesired particles.

Fig. 6. Distribution in χ^2 values obtained in fitting K, Λ, and $\bar{\Lambda}$ decays. If errors were correctly estimated, the average value of χ^2 should be 3.

Fig. 7. Distribution of χ^2/n values obtained in fitting production vertices of $\bar{p} + p \rightarrow \bar{\Lambda} + \Lambda$, $\pi^- + p \rightarrow K^o + \Lambda$, and $\pi^- + p \rightarrow K^o + \Sigma^o$. Information on neutrals from fitted V decays was passed on to the production vertex. The quantity n is the number of degrees of freedom; hence the expected value of χ^2/n is 1.

Fig. 8. Low-momentum background; plot of laboratory angle vs momentum for lambdas produced by the reaction $\pi^- + p \rightarrow K^o + \Lambda$, $\pi^- + p \rightarrow K^o + \Sigma^o$, $\pi^- + p \rightarrow K^o + \Lambda + \pi^o$. The $K^o + \Lambda$ and $K^o + \Sigma^o$ production curves were plotted for a pion momentum of 1.47 Bev/c (the average momentum of the pion at the point of interaction); the shaded area indicates the possible region for a lambda from decay of a sigma-zero. The scattering of some of the events results from the spread of incident momenta, both from variation of beam momentum and variation of energy loss in the chamber. The solid ellipses represent lambdas from fits for $\pi^- + p \rightarrow K^o + \Lambda$. The curve for $\bar{p} + p \rightarrow \bar{\Lambda} + \Lambda$ at 1.61 Bev/c is plotted for comparison with the background.

Fig. 9. Momentum spectra for antiprotons and for negative pions in the 1.64 Bev/c beam upon entry into the 72-inch hydrogen bubble chamber.

Fig. 10. High-momentum background; plot of laboratory angle vs momentum for pion interactions at 1.94 Bev/c. Curves and plotted points have the same interpretations as in Fig. 8. The curve for $\bar{p} + p \rightarrow \bar{\Lambda} + \Lambda$ at 1.99 Bev/c is plotted for comparison with background events. The curve for $\bar{p} + p \rightarrow \overline{\Sigma^o} + \Lambda$ is also shown.

Fig. 11. Production of antilambda and lambda hyperons by antiproton annihilation. The antilambda scatters from a target proton.

Fig. 12. Possible mechanism for antilambda-lambda production as compared with the process of charge-exchange scattering.

Table I. Summary of χ^2 values and production kinematics obtained by fitting decay and production vertices of antilambda-lambda events. In five cases, both antilambda and lambda decayed through charged modes; in four events, only the antilambda was seen; and in two cases, only the lambda was observed.

Event No.	χ^2 $\bar{\Lambda}$ decay	χ^2 Λ decay	χ^2 Prod.	P_{inc} (Mev/c)	P_Λ (Mev/c)	θ_Λ (deg)	$P_{\bar{\Lambda}}$ (Mev/c)	$\theta_{\bar{\Lambda}}$ (deg)	Θ_Λ^{cm} (deg)
1	2.0	6.7	4.7	1615 ± 3	720 ± 5	20.1 ± 0.3	971 ± 6	14.8 ± 0.2	113.5
2	0.91	2.5	9.6	1603 ± 6	1111 ± 8	3.2 ± 0.2	497 ± 3	7.2 ± 0.4	13.8
3	0.01	0.97	no inc. track	none	993 ± 11	-	714 ± 16	-	-
4	18	3.1	6.7	1646 ± 8	1157 ± 12	5.9 ± 0.2	509 ± 4	13.5 ± 0.4	23.9
5	18	4.6	1.7	1620 ± 4	1049 ± 7	11.4 ± 0.3	627 ± 4	19.3 ± 0.3	49.3
6	2.9		2.1	1580 ± 6	1006 ± 11	10.2 ± 0.3	616 ± 5	16.7 ± 0.6	47.1
7	17		0.23	1615 ± 11	590 ± 11	17.8 ± 0.4	1068 ± 20	9.7 ± 0.7	138.1
8	8.3		5.7	1616 ± 9	899 ± 15	17.3 ± 0.3	804 ± 8	19.4 ± 0.4	81.3
9	14		0.25	1604 ± 8	949 ± 13	14.9 ± 0.1	729 ± 7	19.5 ± 0.4	68.8
10		18.1	4.5	1688 ± 18	1046 ± 26	16.2 ± 1.4	745 ± 13	23.2 ± 0.3	66.1
11		12	9.1	1545 ± 4	790 ± 11	15.3 ± 0.5	808 ± 15	14.9 ± 0.3	92.2

Table II. Summary of Beam Characteristics

	Low Momentum	High Momentum
Energy of protons incident on Bevatron Target	6.2 Bev	6.2 Bev
Antiproton beam		
Momentum (at target)	1.64 Bev/c	2.02 Bev/c
Momentum (center of 72 in. Bubble Chamber)	1.61 Bev/c	1.99 Bev/c
Momentum bite (at Bubble Chamber)	±.020 Bev/c	±.030 Bev/c
Solid angle	0.20 millisterad	0.25 millisterad
Production angle (relative to internal proton beam)	1 ± 1 deg	11 ± 1 deg
Transmission of total system	0.33	0.10
Average $\bar{p}$ flux per picture	0.8	0.15
Target		
Material	Al	same
Size	5 in. azimuthally 1/2 in. radially 1/8 in. vertically	same
Physical position - Radius to outside edge	599.4 in.	596.0 in.
Azimuth (NW quadrant-measurement from West tangent tank)	22.34 deg	23.65 deg
Distance from Q entrance	190 in.	180 in.
Virtual position - (distance from principal Plane of Q1)		
- Horizontally	600 in.	350 in.
- Vertically	230 in.	230 in.

Table II. Summary of Beam Characteristics (Cont'd)

	Low Momentum	High Momentum
Separation		
Spectrometer characteristics -		
Plate length	19 ft.	19 ft.
Width of uniform field	6 in.	6 in.
Plate spacing	2 1/2 in.	2 1/2 in.
Average operating voltage	385 kv	385 kv
$\frac{1}{p} \Delta \frac{1}{\beta}$ parameter	.092 $(Bev/c)^{-1}$	0.053 $(Bev/c)^{-1}$
Average angular separation	3.1 mrad	1.8 mrad
Image widths W (vertical) at slits (1st/2nd/3rd systems)	0.20/0.18/0.4-in.[a]	
Magnification (vertical) per stage	1.2/1.0/1.0	
Separation S per stage	0.5/0.40/0.40-in.	
W/S	0.40/0.45/1.0[a]	
Pion/antiproton ratios at target	20,000/1	30,000/1
-at 72-inch Bubble Chamber	0.36/1	1.6/1
Rejection ratio for pions		
System 1	50	
System 2	100	
System 3	10[a]	
Total	5×10^4 [b]	2×10^4 [b]
Beam Composition and total flux		
Average beam composition at Bubble Chamber $(\bar{p}/\pi^-/\mu^-/K^-)$	1.0/0.36/2.8/0.015	1.0/1.8/1.8/0.015
Total number of antiprotons thru chamber	46,000	12,500
Number of antiproton interactions	20,900	5,600

[a] At conclusion of 1.65 Bev/c run, it was found that Q5 had a misplaced pole tip. After this condition was corrected, a good image was obtained at the third slit in the 2.00 Bev/c run.

[b] This rejection ratio is based on all visible pion background in the chamber. Much of the pion background actually has a lower momentum than the anti-proton beam proper.

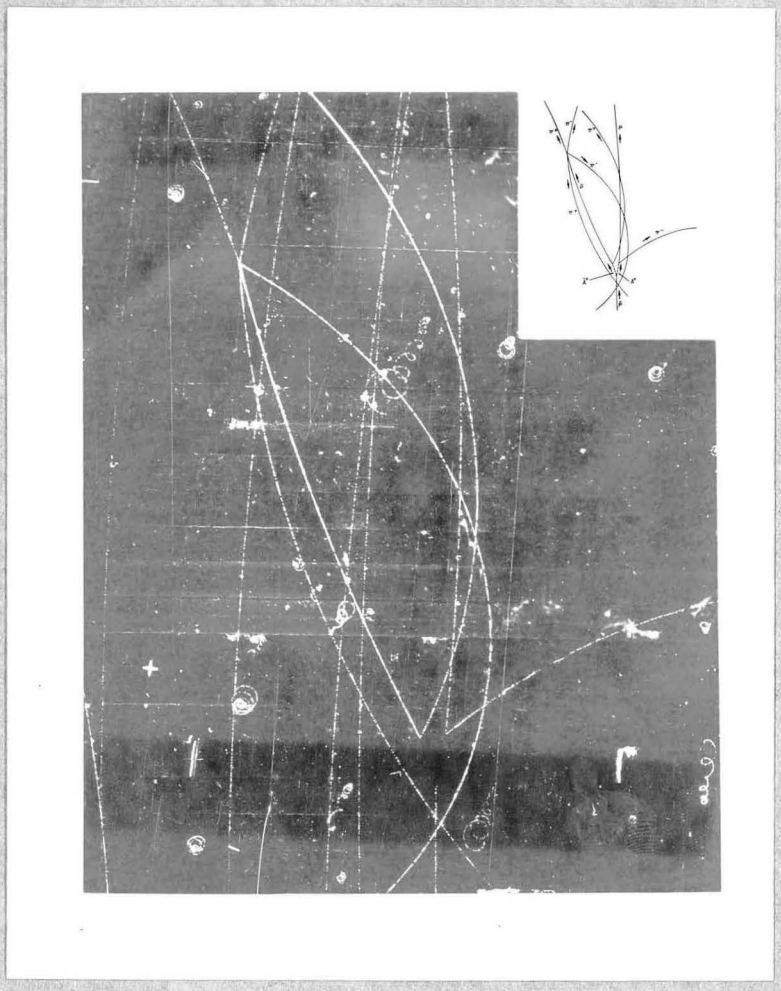

FIG. 1

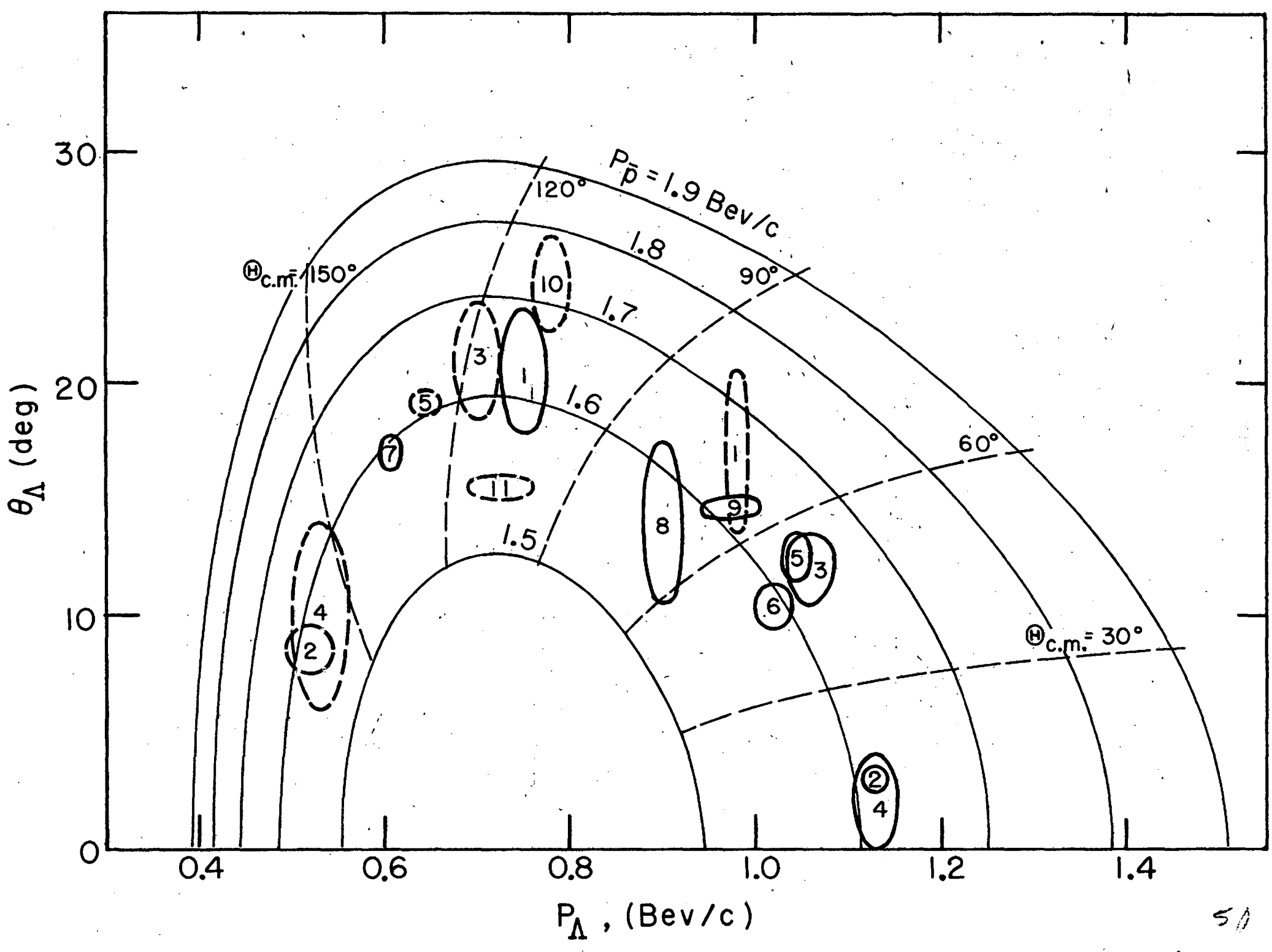

5D

FIG. 2
5B029-1

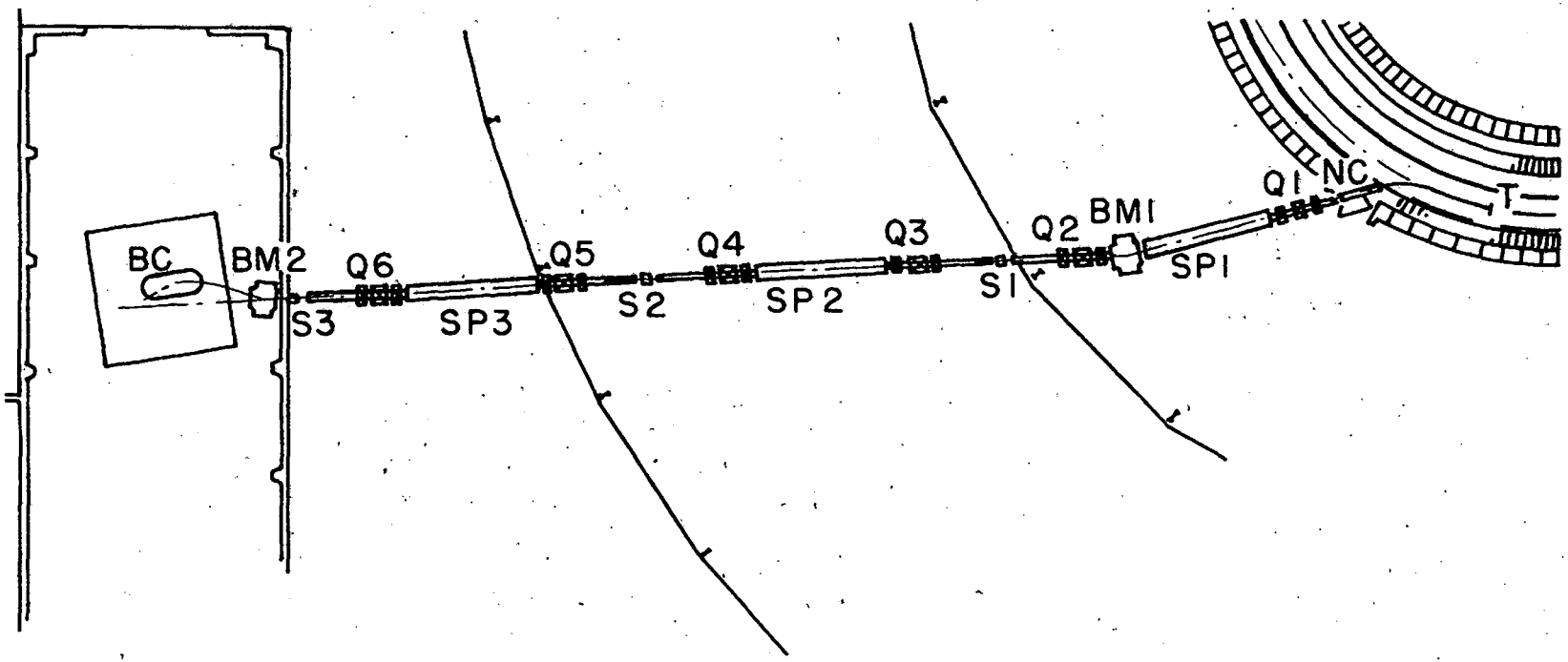

fig. 1

FIG 3
58013-1

Antiproton experiment with 72-in bubble chamber beam optics

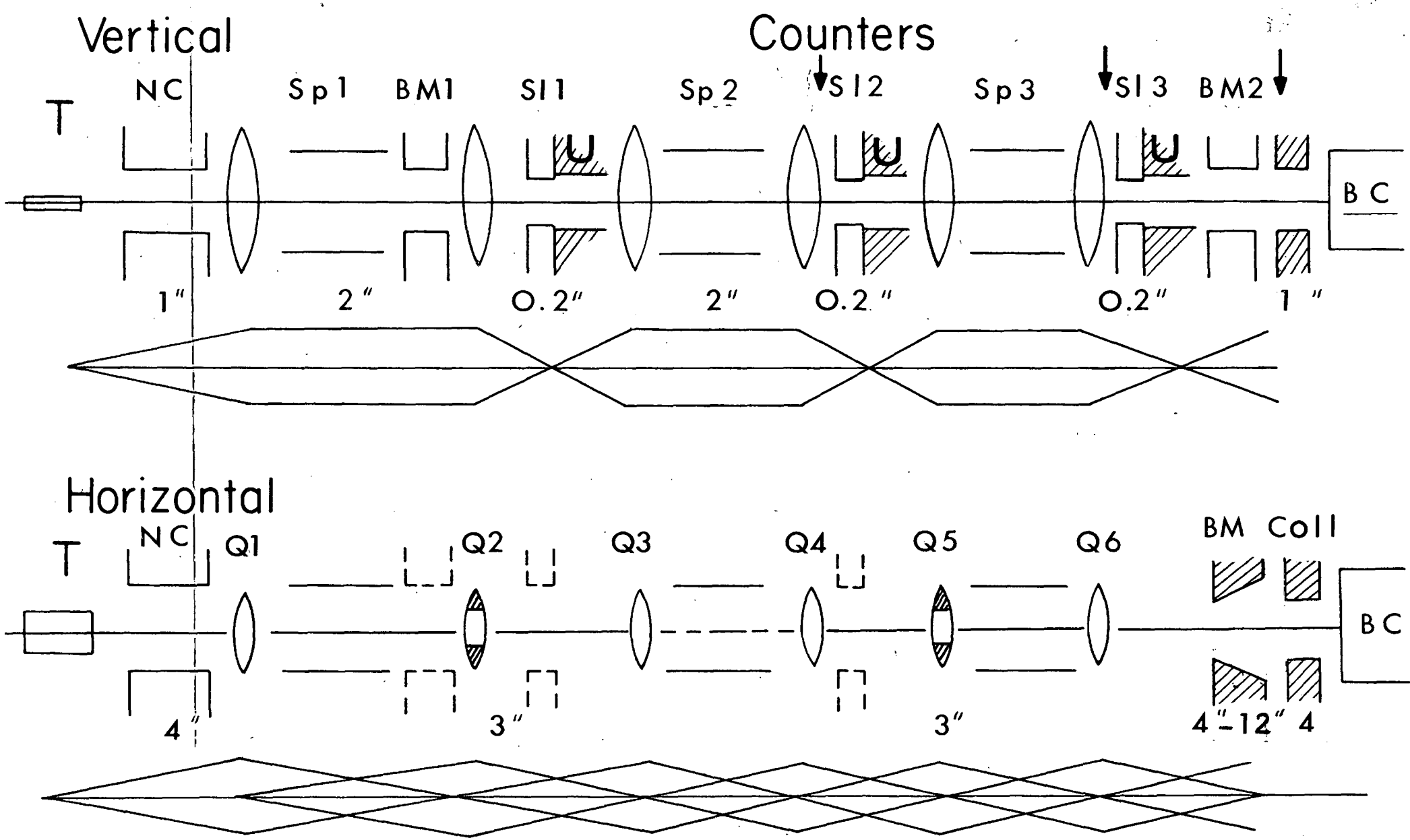

FIG. 4

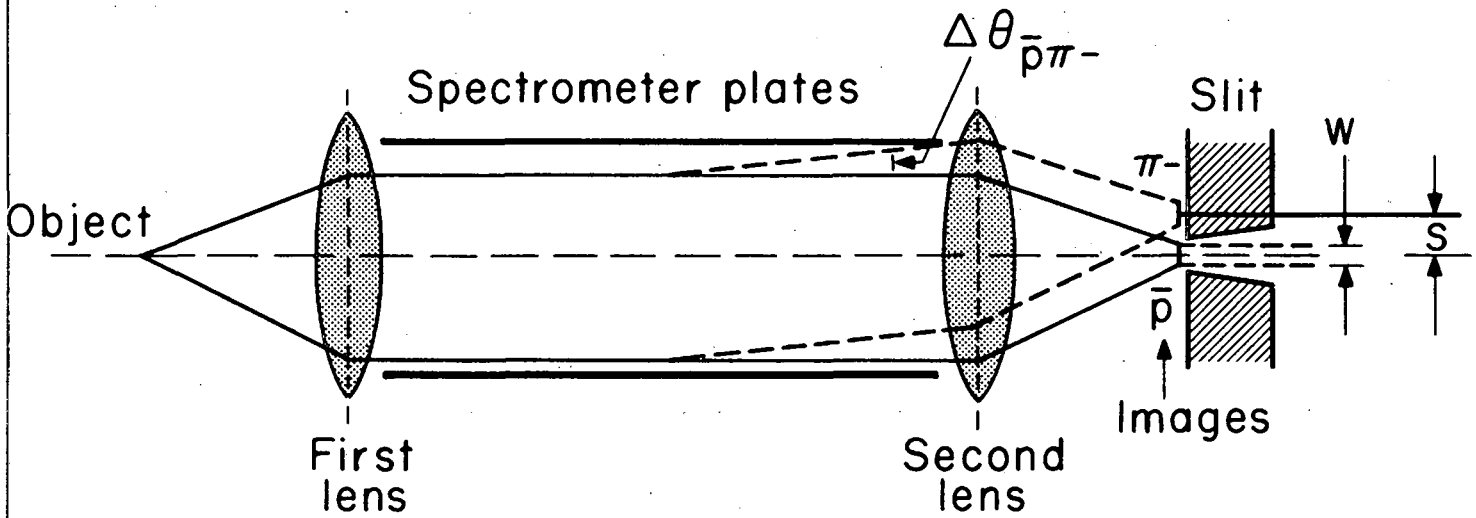
$\Delta\theta_{\bar{p}\pi^-}$
Spectrometer plates
Slit
W
π^-
Object
S
$\bar{p}$
Images
First lens
Second lens

Fig. 5
58141-1

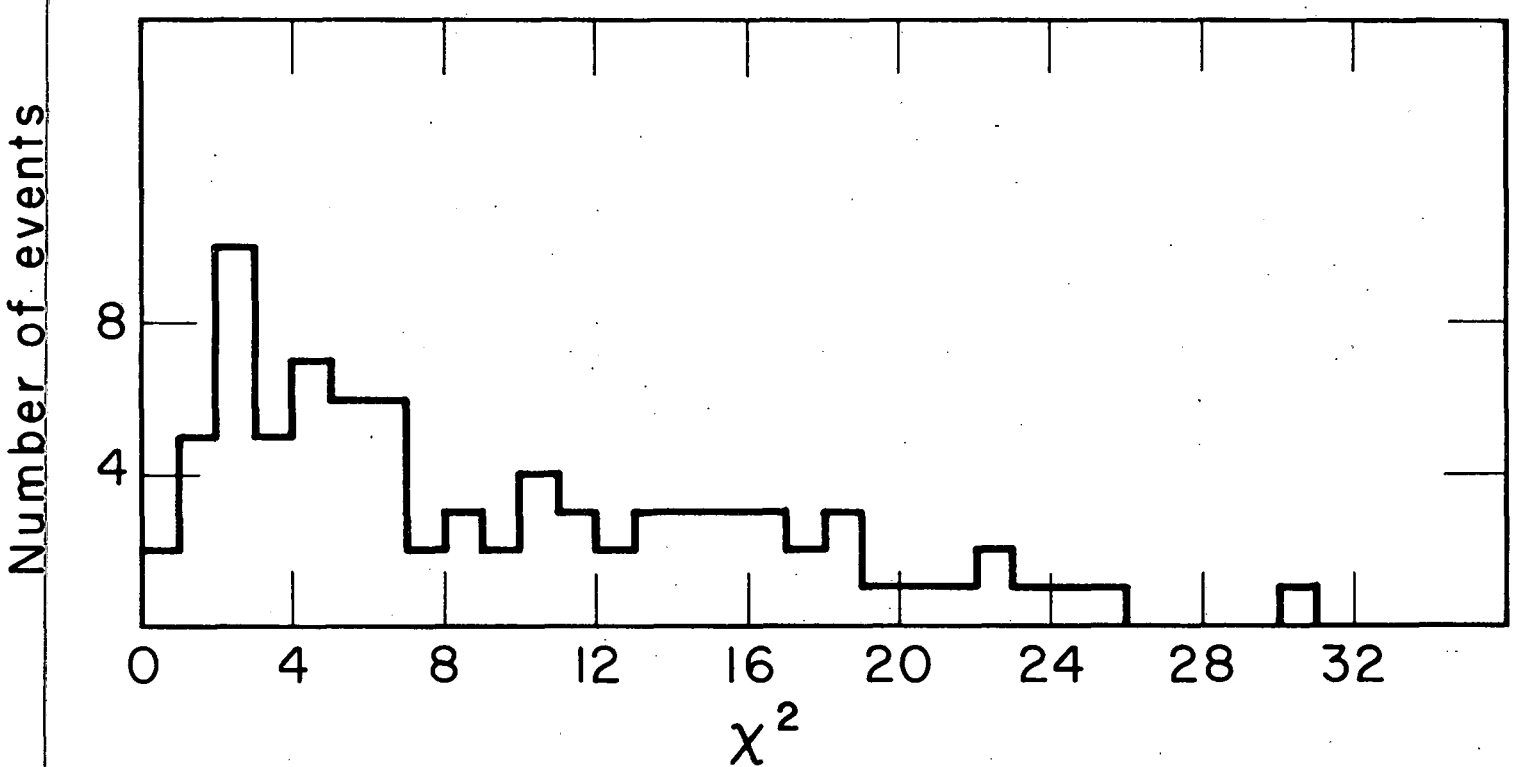

FIG 6
58.142-1

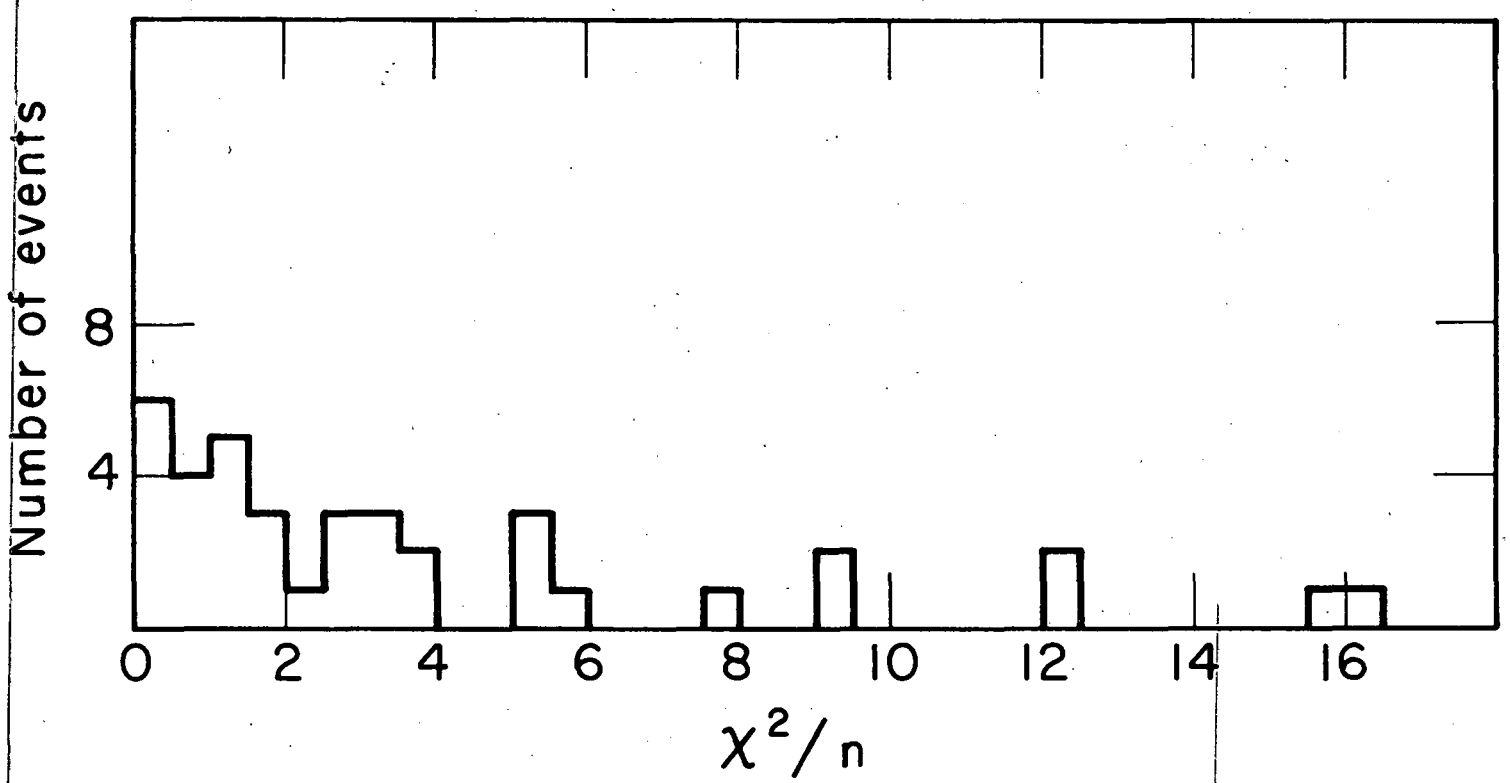

Fig 7
58143-1

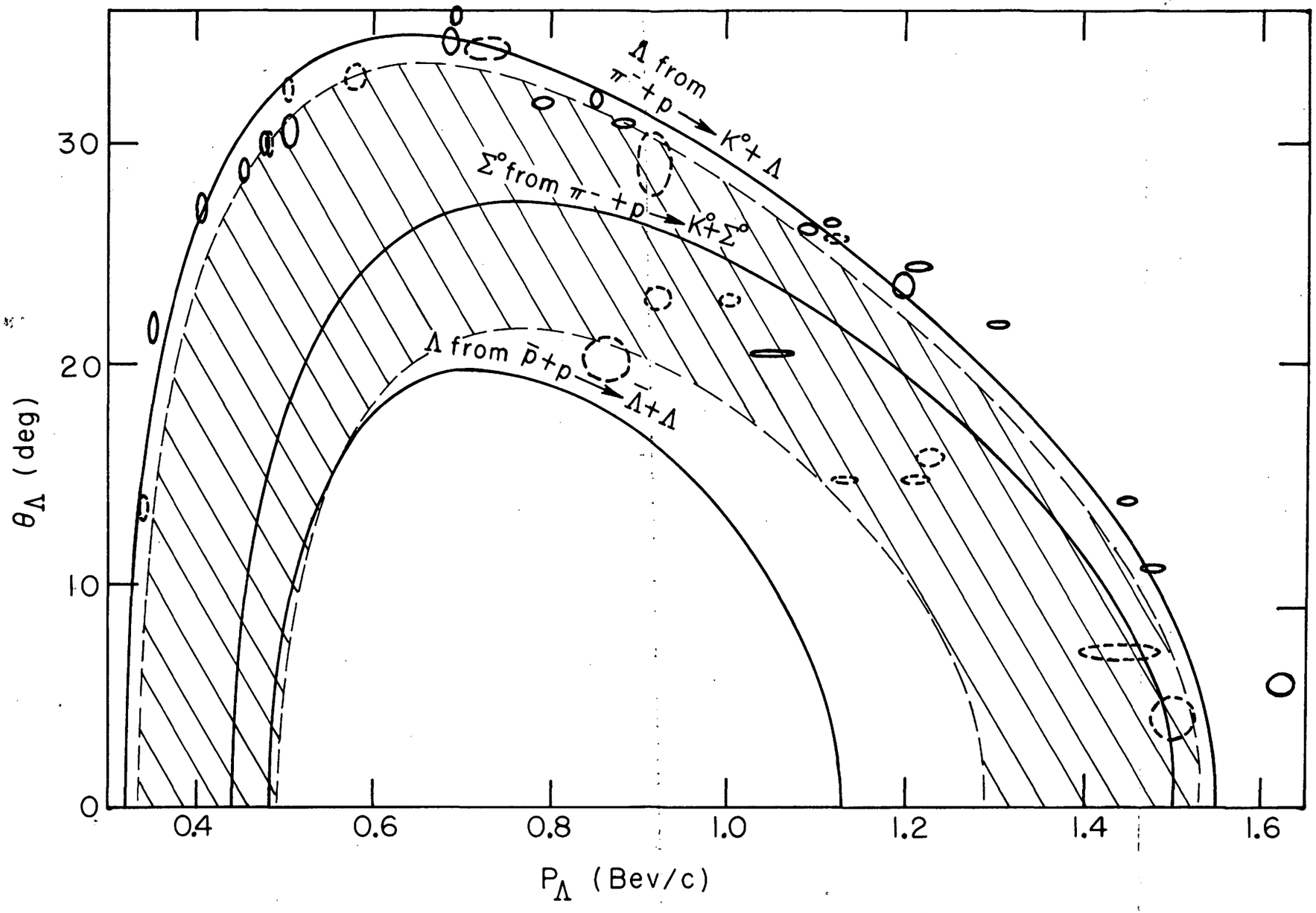
Λ from π⁻+p → K°+Λ
Σ° from π⁻+p → K°+Σ°
Λ from p̄+p → Λ̄+Λ
θΛ (deg)
PΛ (Bev/c)
0
10
20
30
0.4
0.6
0.8
1.0
1.2
1.4
1.6

Fig. 8

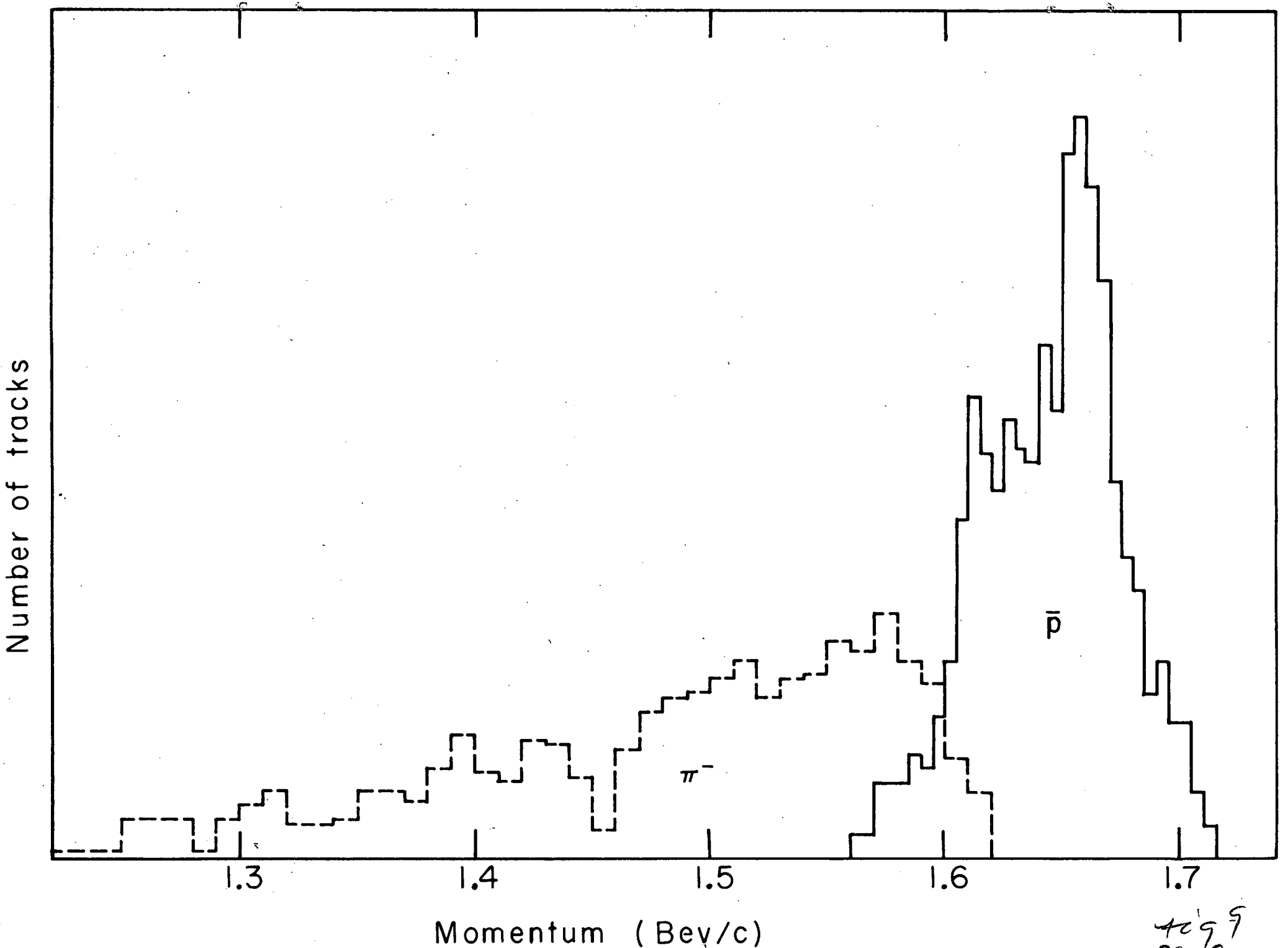

Fig 9
V-8029-1

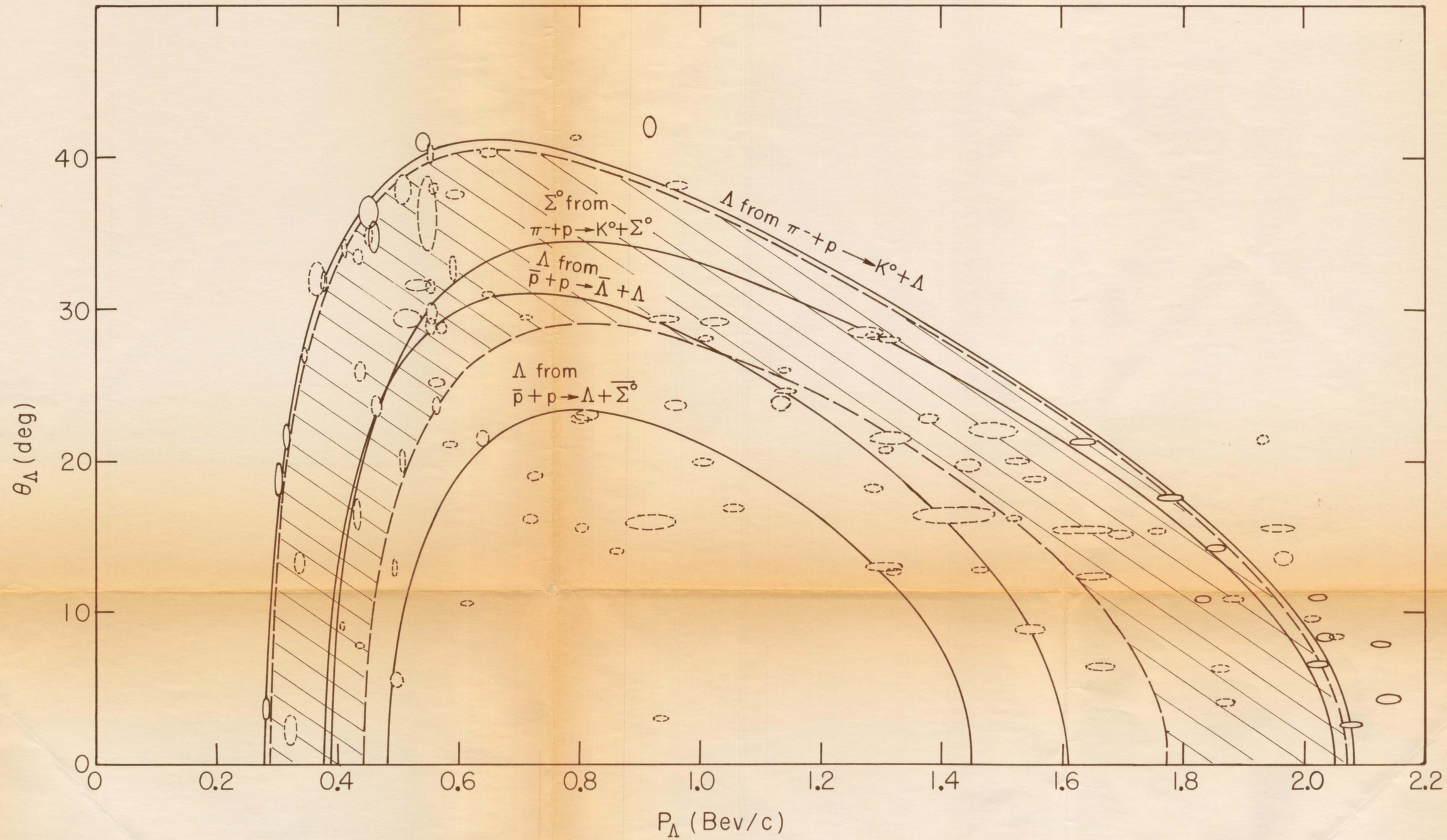
0
40
30
20
10
0
θ_Λ (deg)
Σ° from
$\pi^- + p \rightarrow K^\circ + \Sigma^\circ$
Λ from $\pi^- + p \rightarrow K^\circ + \Lambda$
$\bar{\Lambda}$ from
$\bar{p} + p \rightarrow \bar{\Lambda} + \Lambda$
Λ from
$\bar{p} + p \rightarrow \Lambda + \bar{\Sigma}^\circ$
0
0.2
0.4
0.6
0.8
1.0
1.2
1.4
1.6
1.8
2.0
2.2
P_Λ (Bev/c)

Fig. 1°
GB407-3

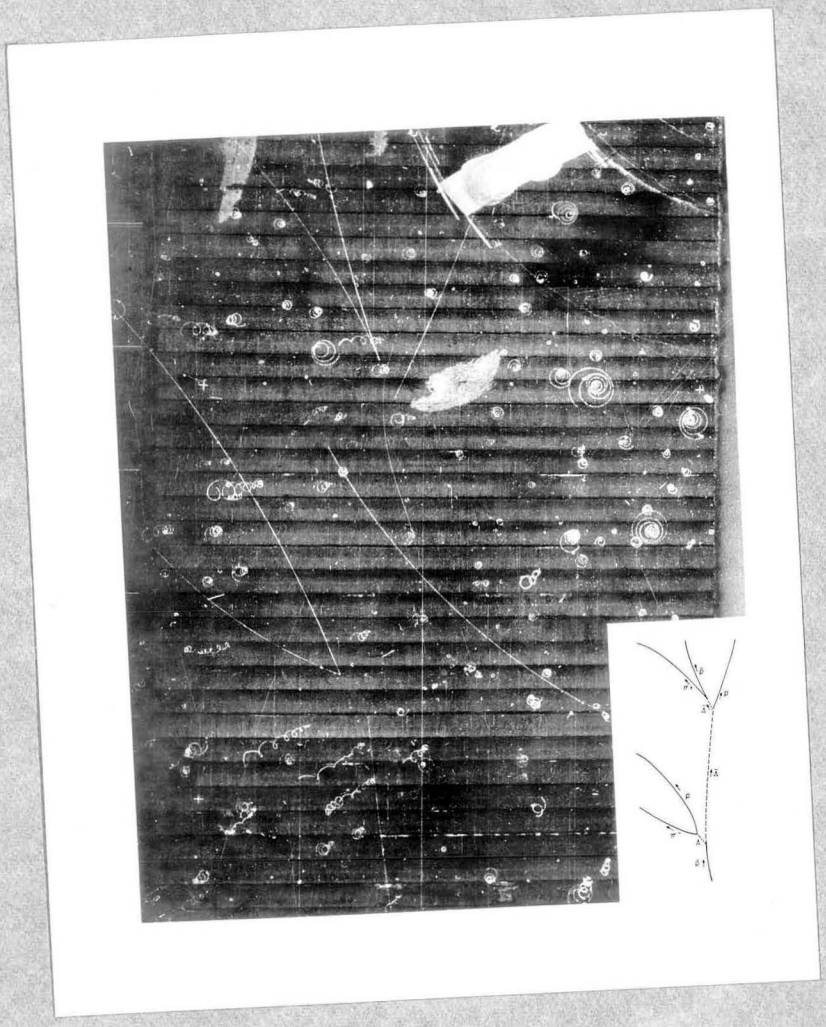

FIG. 11

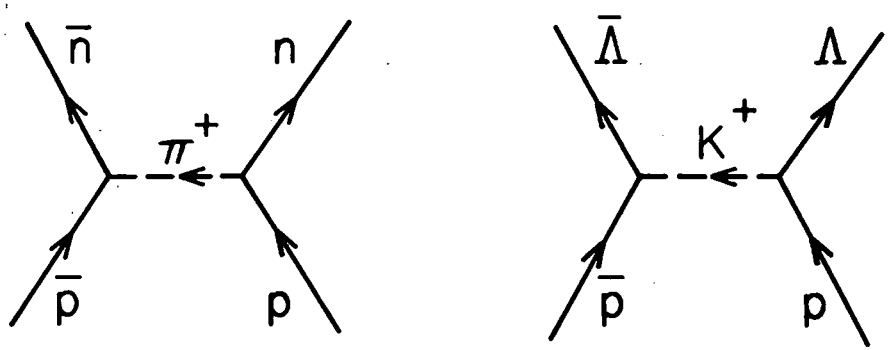

FIG. 1
58144-1